Numerical Investigation of the Optimum Placement Locations of Optical Fiber Bragg Grating Sensors for the Health Monitoring of Bonded Composite Repairs

*G. Tsamasphyros, G. N. Kanderakis, C. Vrettos, K. Kalkanis**

Summary: the use of optical Fiber Bragg Grating sensors (FBG) embedded into composite laminates has proven to be an efficient way for the monitoring of the strain field inside composite laminates. The current work focuses on the use of such sensors for structural health monitoring of bonded composite repairs, often used in the aerospace as well as in the maritime industry. In such applications, the embedding location of the FBG sensors is of great importance, since apart from general strain measurements of the composite, they provide the ability of detecting whether a crack has propagated in the metal or a debonding has occurred between the metal and the composite. Within the current work, a representative case of bonded composite repair of a cracked metallic structure is examined and a series of 3D elasticity linear static finite element models are developed. Various crack lengths and patch disbond sizes have been studied while varying strain distributions were recorded along numerous paths inside the structure. Having recorded and analyzed these strain distributions, certain guidelines have been derived concerning the optimum FBG placement inside the patch, in order to ensure efficient structural health monitoring.

Keywords: adhesive debonding; bonded composite repair; FEA; fiber bragg gratings sensors; structural health monitoring

Introduction

The generation of damage in service is an inevitable, natural characteristic of the aeronautical/maritime structures, which may significantly affect their integrity and safety. The reasons liable for causing damage in a structure are numerous. In many cases, full replacement of a structural element or part is not financially justified, thus leading to the necessity of repair. Consequently, design, analysis and repair technology constitute an ongoing challenge. The current work focuses on cracked metallic skin configurations, repaired by means of bonded composite patches (instead of riveted metallic ones). *Baker*[1,2] has summarized the benefits of these repairs to be: a) increased stiffness achieved with minimum thickness, b) smooth transfer of stresses from the patch to the structure and vice versa, c) decrease of the stress intensity factor and d) optimization of the remaining life in service. Figure 1, illustrates the basic characteristics of the bonded composite repair methodology.

Chue et al.[3] investigated fibre orientation for an inclined crack situation in a biaxially loaded plate using 3D FEA with 20-noded brick elements. They recommend the fibre direction to coincide with the direction of maximum tensile load for double-sided patches and perpendicular to the crack surface for single-sided patch repairs.

The National Technical University of Athens, Faculty of Applied Sciences, Dept. of Mechanics-Lab. of Strength Materials, Zographou Campus, Theocaris Bld., GR-0157 73, Athens, Greece
k_kalkanis@hotmail.com

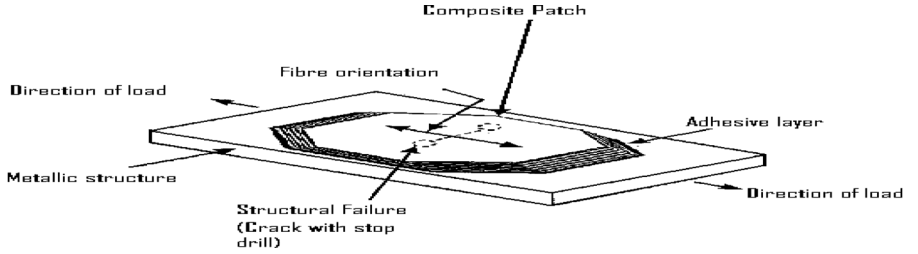

Figure 1.
Bonded composite repair of a thin metallic structure.

In order to enable on line monitoring of the local stress field into a composite patch during the expected cracked propagation, optical fiber sensors can be structurally integrated into it. Fiber optic sensors present significant advantages, compared to other techniques in the area of stress-strain monitoring.[4–10] In[11] the efficiency and the effects of embedding optical fibers in different layers was studied, for the case of crack perpendicular to the loading axis. It has been concluded that the best position to embed optical fibers through-the-thickness of a laminated patch coincides to its neutral surface.[12] In,[13,14] a number of 3D finite element models with optical fibers simulated as one-dimensional spar elements were created, in order to select the appropriate optical fiber paths and the locations of the Bragg Grating sensors for the efficient monitoring of crack propagation and adhesive debonding. Finally, in[15] the increased sensitivity obtained from embedded optical sensors has been quantified, according to the sensors vertical distance (i.e. through the thickness of the composite patch) from the area of interest, in order to proceed with further experimental exploitation.

This paper examines a thin metallic plate with an inclined crack, repaired by means of a bonded composite patch and intends to investigate the optimum placement of an optical sensor into the composite patch (i.e. lengths d_x and d_y from the crack tip, Figure 2) in order to enable sensing changes of strains due to crack propagation or partial patch debonding.

Model Description

As an aircraft skin representative repair case, an 300×80 mm $\times$ 2.5 mm Al 2024T3 orthogonal cracked strip was assumed, containing a 10 mm inclined crack at an angle of 60° compared to the direction of the primary load (i.e. 30° compared to the x axis), as shown in Figure 2.

The specimen is assumed to be placed on a tension device and loaded at 100 MPa uniform tensile stress at its extremities. For the repair of the crack a Textron 5521 Boron Epoxy pre-preg patch was assumed to be bonded. The patch with dimensions 80×80 mm, is composed of 4 plies of pre-preg, having a thickness of 0.125 mm each and a $[45/-45]_s$ fibre orientation. The composite patch is bonded by means of FM73 Epoxy adhesive (0.13 mm thickness after curing). The mechanical properties of the materials used are presented in Table 1. The optical fibre was not modelled in this phase, as the primary concern of this work is the quantification of the strain distribution.

Several configurations have already been studied being subject to uniaxial loading. This particular configuration was selected so as to investigate a more complicated situation (uniaxial loading with an inclined crack) and may simulate a damage caused by external reasons (e.g. corrosion, impact). In total, 6 models of the repaired patch were created using finite elements. The first model refers to a repaired specimen with no debonding. The remaining models were created assuming

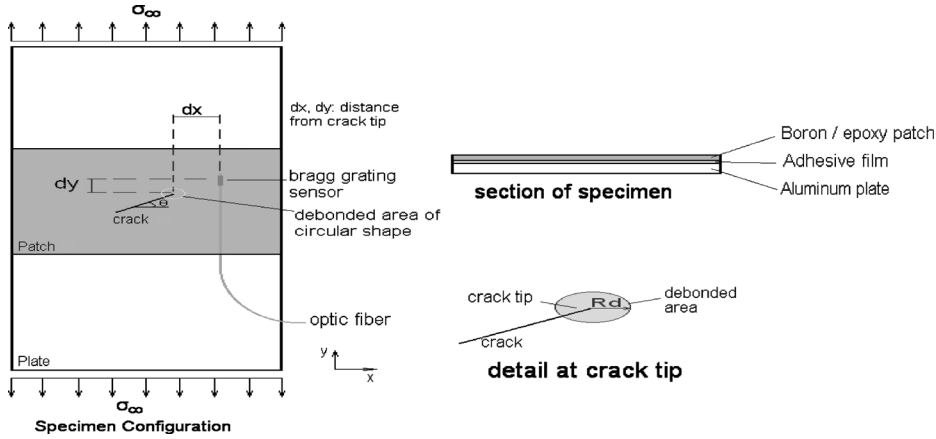

Figure 2.
Specimen geometry.

a debonding at the right crack tip of a radius $R_d = 0.5$, 1.0, 1.5, 2.0 and 2.25 mm respectively so as to determine the strain distributions inside the patch for each debonding, under the same load. Furthermore, two models representing the unrepaired specimen were created, the one using plane elasticity elements and the other applying 3D elasticity elements, in order to compute the Stress Intensity Factor (SIF) without a repair, for comparison with the repaired specimen purposes. Figure 3 shows a representative FE model created within this study, indicating the layers used for the modeling of each material.

For the modeling of the cracked unrepaired specimen (2D model) 8-node four sided PLANE 82 ANSYS plane stress elements were used.[16] In the case of the 3D models, for the aluminium and the adhesive 20-node six sided SOLID 95 3D elasticity elements were used, whereas for the multilayered patch 20-node LAYERED191 layered hexahedral elements were created.[16] The crack (10 mm) in the aluminium was modeled as a straight line, along which no continuity of elements exists on either sides. The crack tip was modeled with 16 prismatic singular elements placed circumferentially to it (Figure 4). In the case of the 2D model the elements are collapsed to singular triangular elements, by moving the nodes at ¼ of the length of the elements side. The debonding between the adhesive and the aluminium was modeled as a circular area of radius R_d, with its center at the crack tip. At this area no connection between elements of the adhesive and the patch exists. The specimen is assumed to be loaded by a tension device, so the displacement u_z was

Table 1.
Mechanical properties of materials used.

Aluminium 2024-T3	Young's modulus (E)	72.4 GPa
	Poisson ratio (v)	0.3
Adhesive	Young's modulus E	3.5 GPa
	Poisson ratio (v)	0.3
Boron/Epoxy Textron 5521	Young's modulus E_{11}	210 GPa
	Young's modulus E_{22}/E_{33}	10 GPa
	Shear modulus G_{12}	4.5 GPa
	Shear modulus G_{13}/G_{23}	3.5 GPa
	Poisson ratio v_{12}	0.21
	Poisson ratio v_{13}/v_{23}	0.019

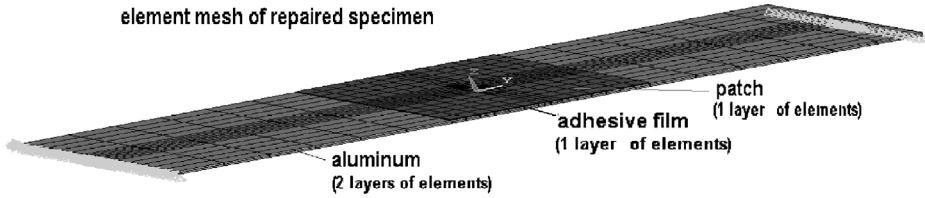

Figure 3.
Finite element model of the repaired specimen.

restrained at the model edges, while at the same points uniform tensile stress of $\sigma_{yy} = 100$ MPa was applied.

Numerical Results

As the dominant sensing direction coincides with the optical fiber longitudinal axis, the most interesting result would be the strain/deformation ε_{yy} at the direction of the optical fibre as it is the key parameter for debonding. Moreover, the corresponding calculated SIF are presented in Table 3. The SIF for mode I, after the addition of the patch, is reduced on the mean surface and the upper side of the metallic specimen by 22.68% and 59.06%, respectively (Table 2). However, the neutral surface in no longer on the same plane, with the plane of loading and as a result the applied tension induces out of plane bending (Figure 5). Due to this, the lower side of the specimen receives additional tensile loads, a fact which consequently opens the crack furthermore.

Taking into consideration the effects of debonding, the SIF at the side of the patch increases monotonously with the increase of the debonding magnitude, for both modes considered, as graphically illustrated in Figure 6.

In contrast to the upper surface, at the lower surface of the specimen, where there is no patch, the variation of SIF to the debonding magnitude is not monotonous (Figures 7–8).

As presented in the diagram, the SIF is initially slightly reduced, for both modes, and then starts increasing monotonously. This temporary change of the SIF occurs due to the reduction of the patch induced bending effects, created by the single sided patch, as its efficiency has been decreased due to debonding. However, this relief of the SIF is temporary, as with further debonding bending may be decreased, but the patch is no longer efficient at the crack tip and as a consequence the SIF increases.

Optimum Placement of Optical Sensors

The basic purpose of this study is to identify the position at which the optical sensors should be placed, so as to diagnose changes at the repaired structure (e.g. crack propagation or adhesive debonding). To enable this, the sensors must be situated at points that present significant variations in strain upon loading. For the examined case,

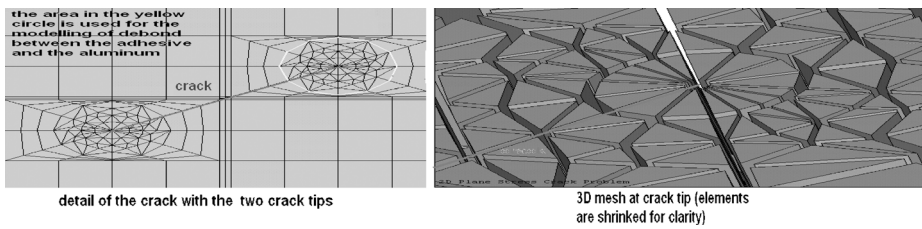

Figure 4.
Detailed mesh at the crack region.

Table 2.
Stress intensity factors (N/mm$^{3/2}$), calculated by ANSYS.

Position	mode	2D with crack	3D with crack	3D with repair	% difference with- without repair (3D models)
Lower side z = 0	I	346.40	329.50	358.38	8.76
	II	2.7465	1.8989	53.211	2702.20
Mean surface z = t/2	I	346.40	333.31	257.71	−22.68
	II	2.7465	11.688	10.462	−10.489
Upper side z = t/2	I	346.40	329.50	134.90	−59.06
	II	2.7465	1.8989	38.072	1904.95

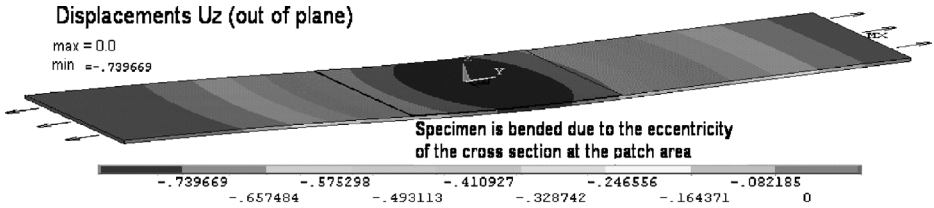

Figure 5.
Bending of the specimen due to non symmetric cross section of the patch area.

distributions of strain ε_{yy} were computed along axes AB and CD, crossing the crack tip (Figure 9), for the same imposed load, while assuming different adhesive debonding magnitudes.

Figures 10–11 present ε_{yy} strains along axis AB and CD respectively, which are developed between the adhesive and ply 1 of the patch, for different debonding cases.

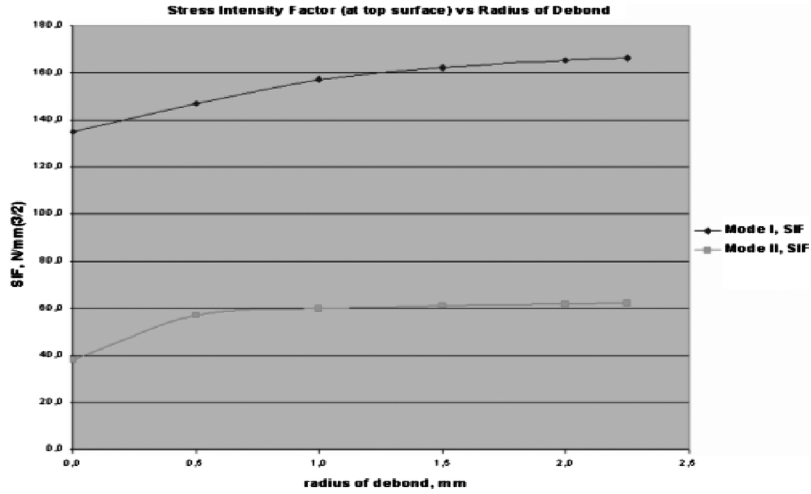

Figure 6.
Variation of SIF, at the patched side, as a function of debonding magnitude.

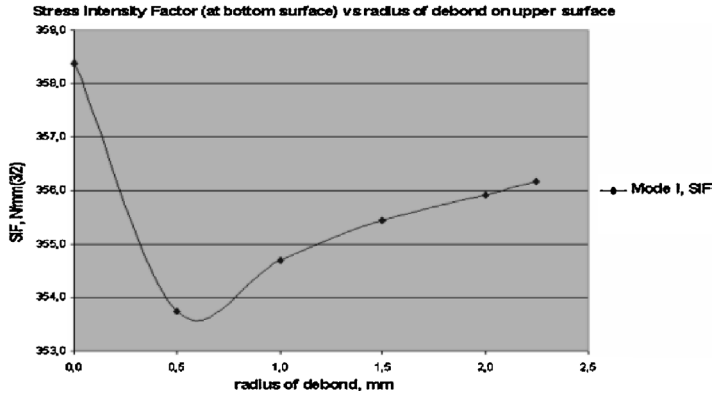

Figure 7.
Variation of the Mode I SIF at the unpatched side, as a function of the debonding magnitude.

In order to achieve a better visualization of the developed strains, the following values have been calculated:

relative strain variation

$$= \frac{\varepsilon_{debond} - \varepsilon_{no\ debond}}{\varepsilon_{no\ debond}} \times 100\% \quad (1)$$

absolute strain variation

$$= \varepsilon_{debond} - \varepsilon_{no\ debond} \quad (2)$$

where ε_{debond} is the strain at a certain point, for a model with a debonding of radius R_d and $\varepsilon_{no\ debond}$ is the strain at the same point for a model with no debonding.

Figures 12 and 13 present the calculated stain values for the case of a repair with a debonding radius of $R_d = 2.25$ mm along axis AB and CD, respectively, for different patch layers.

As presented in Figure 12, absolute strain varies along axis AB in a region of $dx = 5$ mm on both sides of the crack tip (10 mm in total), for points that lie between the adhesive and the 1st layer of the patch and for the points that lie between layers 2 and 3 of the composite patch (blue and pink lines

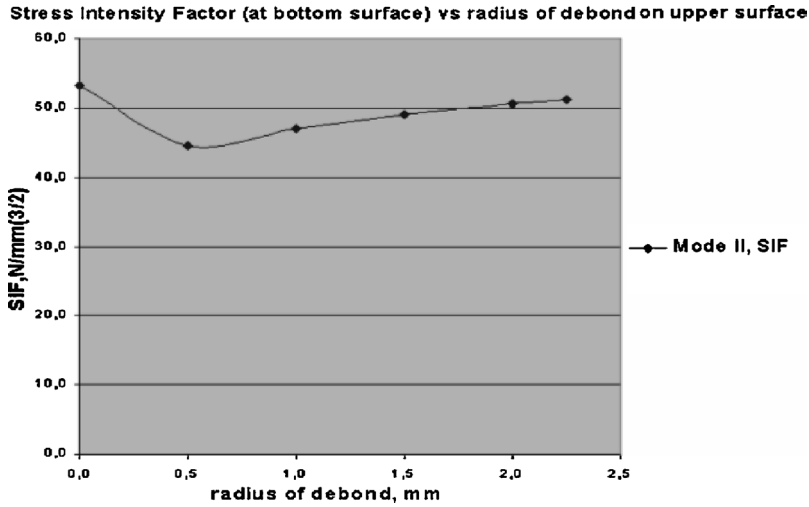

Figure 8.
Variation of SIF for mode II, at the unpatched side, as a function of debonding magnitude.

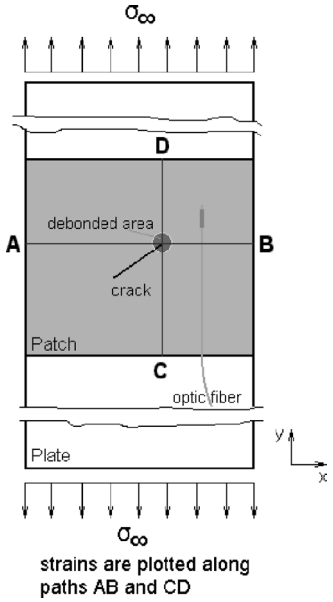

Figure 9.
Definition of axes along which strains have been computed.

respectively). At the upper surface of the patch (i.e. over layer 4) the variation of strain (yellow line) is important in a much narrower region of approximately dx = 2.5 mm, on both sides of the crack tip (5 mm in total). This fact is expected, as at a point which is remote to the debonding area, the effect of such debonding strongly weakens.

Similarly, Figure 13 presents the absolute variation of strain along axis CD. Strain varies in a region of approximately dy = 5 mm on both sides of the crack tip, for the same examined cases (i.e. between adhesive-patch, layers 2–3 and over layer 4).

Consequently, in order for a Bragg grating sensor to "diagnose" the existence of a debonding with radius 2.25 mm between the metal and the adhesive, the sensor should be placed in a radius of maximum 4–5 mm from the crack tip and no more than 2 layers above the adhesive. If the sensor is embedded above the 2nd layer, then it should be placed in a radius smaller than 2–2.5 mm from the crack tip. Finally, according to the results of similar works for different radii of debonding (0.5 mm, 1 mm, 1.5 mm and 2 mm) it was identified that the smaller the magnitude of the debonding, the narrower becomes the region in which the sensor is able to diagnose the magnitude of such debonding.

Conclusions

According to the results of this study, the following conclusions can be drawn:

The Mode I SIF at the upper surface of the specimen is decreased when applying the composite repair, while at the lower surface of the specimen it slightly increases, due to the bending generated because of the non symmetric cross section of the repaired specimen.

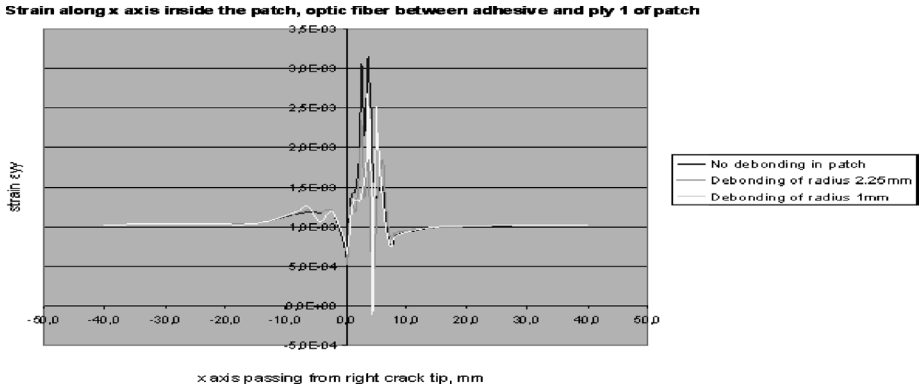

Figure 10.
Strain distribution ε_{yy} along horizontal axis AB.

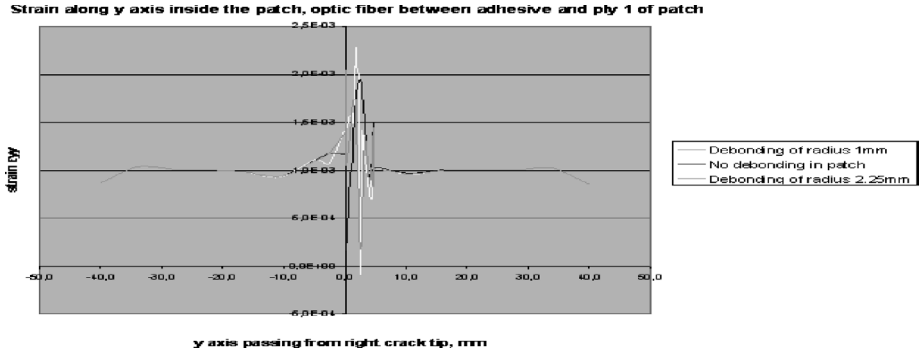

Figure 11.
Strain distribution ε_{yy} along the length of the vertical axis CD.

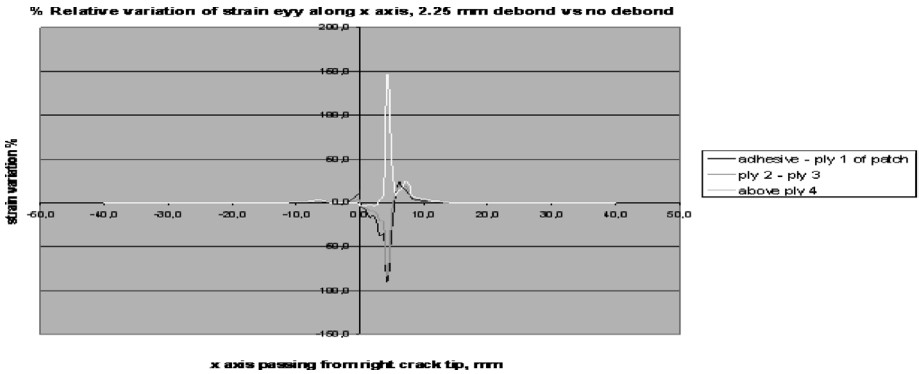

Figure 12.
Relative % strain variation along axis AB for a repair with a debonding of radius 2.25 mm.

On the top surface of the specimen the Mode I SIF increases monotonously with the debonding magnitude, while on the lower surface Mode I SIF decreases for a small magnitude of debonding, due to the decrease of the specimen's bending.

The approximation of the point at which an optical sensor should be placed, to

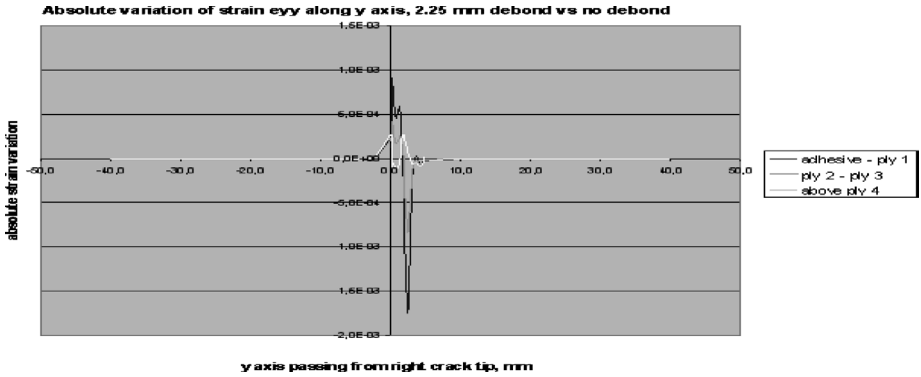

Figure 13.
Absolute strain variation along axis CD for a repair with debonding of radius 2.25 mm.

adequately diagnose a damage with a given magnitude and position, can be performed with the depiction of % relative variations of the mechanical strain, at given axes and planes on a structure. In order for a Bragg grating sensor to «diagnose» a debonding with radius 2.25 mm between the metal and the adhesive, the sensor should be placed in a radius of maximum 4–5 mm from the crack tip and no more than 2 layers above the adhesive layer. If the sensor is embedded above the 2nd layer, then it should be placed within a radius smaller than 2–2.5 mm from the crack tip.

[1] A. A. Baker, Repair of cracked or defective metallic aircraft components with advanced fibre composites. An overview of Australian work, *Comput Struct* **1984**, *2*, 153–81.

[2] A. A. Baker, R. J. Chester, Recent advances in bonded composite repair technology for metallic aircraft components, In: Advanced Composites 93. Chandra T, Dhingra AK, editors. Proceedings of the International, Conference on Advanced Composite Materials, **1993**, p. 45–9.

[3] Ramesh Chandra, M. V. V. Murthy, T. S. Ramamurthy, A. K. Rao, Analytical estimation of stress intensity factors in patched cracked plates, *Engng Fract Mech* **1985**, *21*, 479–94.

[4] G. Kanderakis, The method of repairing metallic structures with Composite Patch Repair, PhD Thesis, National Technical University of Athens, **2000**.

[5] R. Jones, R. J. Callinan, Finite element analysis of patched cracks, *J Struct Mech* **1979**, *7*, 107–30.

[6] C. H. Chue, L. C. Chang, J. S. Tsai, Bonded repair of a plate with inclined central crack under biaxial loading, *Comput Struct* **1994**, *28*, 39–45.

[7] N. Furnarakis, Structural health monitoring of Composite patch repairs, with the use of optical sensors, PhD thesis, National Technical University of Athens, **2005**.

[8] Raymond Measures, ''Fiber Opt. Sens. for Comp. Smart Structures'', AGARD, CP-531, **1992**.

[9] J. Sirkis, et al. ''What do embedded optical fibers really measures?'', SPIE, Vol. 1777, 1992, N. Spon Ltd, **1981**, London & NY.

[10] S. Crossley, Z. Marioli-Riga, G. Tsamasphyros, G. Kanderakis, N. Furnarakis, A. Ikiades, M. Konstantaki, ''Smart Patches: Self-monitoring composite patches for the repair of aircraft'', SPIE's Proc, Int. Symp. on Opt. Tech. for Industrial and Environmental Sensing, Conf. on Intel. Transp. Sensors and Controls, Vol 5272B, Providence, RI, USA, Oct 29–Nov 3 **2003**.

[11] G. J. Tsamasphyros, N. K. Furnarakis, G. N. Kanderakis, Z. P. Marioli-Riga, ''Three-Dimensional Finite Element Analysis of Composite Patches with Embedded Optical Fibres – Through Thickness Optimization'', ICCES 01, Puerto Vallarta, Mexico, 19–24 August **2001**.

[12] L. R. F. Rose, Theoretical Analysis of Crack Patching in A. A. Baker, R. Jones (Ed.), *Bonded Repair of Aircraft Structures*, Martinus Nijhoff Publishers, Dordrecht **1988**.

[13] G. Tsamasphyros, N. Furnarakis, G. Kanderakis, Z. Marioli-Riga, R. Chemama, R. Bartolo '' 3D FEA of Comp. Patches with Embed. Opt. Fibers–Select. of Opt. Fib. & Sensors Locations'', SHM 2002,D.L.Balageas, 1203–1210, Destech Publ,ENS Cachan France, July 10–12, **2002**.

[14] G. J. Tsamasphyros, N. K. Furnarakis, G. N. Kanderakis, Z. P. Marioli-Riga, ''Detection of patch debonding in composite repaired cracked metallic specimens, using optical fibers and sensors'', SPIE Optical Metrology Conference, 23–26 June **2003**, Munich, Germany.

[15] Numerical examination of optical sensors sensitivity through-the-thickness of a bonded composite patch for the detection of crack propagation and adhesive debonding, G. J. Tsamasphyros, G. N. Kanderakis, N. K. Furnarakis, Z. P. Marioli-Riga, 2 nd Proceedings of the 2nd European Workshop on Structural Health Monitoring, Munich, 7–9 July **2004**, pp. 514–524.

[16] ANSYS. *Finite Element Analysis Programme, Elements Manual*, SAS IP Inc., **1998**.

